Desalination and Water Treatment
www.deswater.com

doi: 10.5004/dwt.2017.20729

75 (2017) 26–33
May

Enhanced hydrophilicity and antibacterial activity of PVDF ultrafiltration membrane using Ag_3PO_4/TiO_2 nanocomposite against *E. coli*

Xiaoting Hong[a,*], Yumei Zhou[b], Zhuoliang Ye[c,*], Haifeng Zhuang[a], Wanpeng Liu[a], K.S. Hui[d], Zhi Zeng[b], Xianhuan Qiu[b]

[a]*School of Civil Engineering and Architecture, Zhejiang University of Science and Technology; Key Laboratory of Recycling and Eco-treatment of Waste Biomass of Zhejiang Province, Hangzhou 310023, China, Tel. +86 (0571) 81315186; Fax: +86 (0571) 81315186; emails: hanren.xiaoting@gmail.com, hongxt@zust.edu.cn (X.T. Hong), 286339399@qq.com (H. Zhuang), wpliu@zust.edu.cn (W. Liu)*
[b]*School of Chemistry & Environment, South China Normal University, Guangzhou 510006, China, emails: 844654470@qq.com (Y. Zhou), 415819402@qq.com (X. Qiu), zhizeng@scnu.edu.cn (Z. Zeng)*
[c]*School of Chemical Engineering, Fuzhou University, Fuzhou, Fujian 350116, China, email: yezl@fzu.edu.cn*
[d]*School of Mathematics, Faculty of Science, University of East Anglia, Norwich, NR4 7TJ, UK, email: k.hui@uea.ac.uk*

Received 13 October 2016; Accepted 20 March 2017

ABSTRACT

Ag_3PO_4/TiO_2 nanocomposite was fabricated by an in situ precipitation method and then blended into poly(vinylidene fluoride) (PVDF) casting solution to prepare the ultrafiltration membrane via wet phase inversion technique. The water flux and bovine serum albumin (BSA) rejection rate of membrane were investigated; meanwhile, the ultrafiltration membrane morphologies and structural properties were analyzed using scanning electron microscope (SEM) and X-ray diffraction. Compared with the control membrane, the permeate performance of blended membranes was improved while possessing a steady BSA retention due to enhanced hydrophilicity. Mechanical tests revealed that the modified membranes exhibited a larger tensile strength and breakage elongation. SEM images and the halo zone testing were employed to assess the antibacterial performances of the nanocomposite membranes against *Escherichia coli*. The antibacterial tests confirmed that the modified membranes showed an effective antibacterial property against *E. coli*.

Keywords: Phase inversion; PVDF ultrafiltration membrane; Ag_3PO_4/TiO_2 nanocomposite; Hydrophilic and antibacterial

1. Introduction

As an increasing global demand for water security and more stringent environmental requirements, membrane treatment processes play a significant role in water and wastewater treatment and maintain steady increase over the past few years ascribed to its advantages and specific characteristics such as compactness, high efficiency, ease operation, and low energy consumption [1–3]. In particular, poly(vinylidene fluoride) (PVDF) membrane is broadly employed for the processes of pervaporation, reverse osmosis, microfiltration, and ultrafiltration ascribed to its extraordinary thermal, chemical stability, high mechanical strength, and inertness derived from its fluorinated structure [4,5]. Nevertheless, membrane fouling, which results in unpredictably decreased life span and severe damage of the membranes, is still one of the important threats for PVDF membrane treatment technology because of its intrinsic hydrophobic nature and low surface energy property [1,6,7].

In order to make PVDF membranes less prone to irreversible fouling, lots of efforts have been devoted to improve membrane antifouling property and permeability in addition to the optimization of cleaning methods and operating conditions [8], including material modification, polymer blend,

* Corresponding author.

and surface modification [9,10]. Among them, blending modification by incorporation inorganic nanomaterials to synthesize nanoparticle-functionalized membranes has become a great interest for manufactures and researchers [11–13]. The blended membranes normally achieve the desired enhancement of separation properties since the resultant nanocomposite membranes simultaneously possess comprehensive characteristics of the blended nanomaterials and matrix membrane materials. Currently, many researchers have focused on Al_2O_3, SiO_2, and TiO_2 nanoparticles as blending materials for PVDF surface modification [14–16]. Among them, TiO_2 nanoparticles have achieved great attention due to the high hydrophilicity, excellent chemical stability, and potential antifouling abilities [17–19].

A large number of studies have investigated the influences of TiO_2 blending on the enhancement of PVDF membrane properties. Cao et al. [20] reported the effects of TiO_2 nanoparticle size on the separation behavior and morphology of PVDF membrane, and suggested nanosized TiO_2 with 10 nm for blending modification. Damodar et al. [21] investigated the impacts of different dosages of TiO_2 nanoparticles in the PVDF dope on their antibacterial and antifouling behaviors, and found that good hydrophilicity of membrane was established by adding low concentration of TiO_2 into the PVDF casting solution. Oh et al. [22] modified PVDF-UF membrane with TiO_2 nanoparticles and found that the antifouling capability of the nanocomposite PVDF membranes was significantly improved. Normally, blending TiO_2 nanoparticles greatly influenced the porosity and surface hydrophilicity of the nanocomposite membrane, and thus, the flux and permeability of TiO_2 blended PVDF membrane was improved [23]. Compared with the unmodified PVDF membrane, incorporation of TiO_2 nanoparticles into membrane matrix could also show better antibacterial and antifouling capabilities upon UV light irradiation [23]. Bacteria are the major microorganisms that lead to severe membrane fouling and irreversibly deteriorate membrane performance. To alleviate the bacteria induced membrane fouling during membrane filtration processes, it is vitally important to ensure the membrane possessing an antibacterial property [24]. Therefore, an effective strategy is usually proposed to add inorganic antibacterial agents such as silver nanoparticles or Ag-loaded nanocomposites.

In this study, an Ag-loaded TiO_2 nanocomposite (Ag_3PO_4/TiO_2) was successfully blended into casting solution to improve the antifouling behavior and surface hydrophilicity of the PVDF nanocomposite membrane via the wet phase inversion process. The support of TiO_2 and loading material of Ag_3PO_4 nanoparticle were expected to substantially promote the surface hydrophilicity, mechanical strength, and antibacterial behaviors of the as-synthesized PVDF nanocomposite membranes. The influence of the different dope solution composition on the structural properties and separation performances of the resultant nanocomposite membranes were comprehensively explored with respect to bovine serum albumin (BSA) rejection ratios, pure water flux, surface morphologies, surface hydrophilicity, tensile strength, porosity, and fouling resistance. The antibacterial property of Ag_3PO_4/TiO_2 blended nanocomposite membrane was revealed by the adhesion of *Escherichia coli* bacteria to membranes and halo zone testing.

2. Materials and methods

2.1. Materials

All reagents were used without further purification. FR-904 PVDF was purchased from Shanghai 3F New Material Co., Ltd. (Shanghai, China). It was dried at 100°C overnight in a vacuum oven prior to use for dope solution. Commercial TiO_2 (Degussa P25, Germany), silver nitrate (99.8%), polyvinyl pyrrolidone (PVP, K-30), ethyl alcohol (99.7%), sodium chloride (99.5%), *N*,*N*-dimethyl formamide (DMF), trisodium phosphate, anhydrous disodium hydrogen phosphate, anhydrous sodium hydrogen phosphate, glutaral dehyde, and isoamyl acetate were supplied by Shanghai Aladdin Bio-Chem Technology Co., Ltd. (Shanghai, China). Nutrient agar, yeast extract, and peptone were provided by Shanghai Bluetech (Shanghai, China) and Beijing Aoboxing Biotechnology Co. Ltd. (Beijing, China), respectively. A Millipore Milli-Q Advantage A10 system was used to produce the deionized (DI) water. *E. coli* DH5α was provided by Sun Yat-sen University (Guangzhou, China).

2.2. Preparation of Ag_3PO_4/TiO_2 nanocomposite

The immobilization of Ag_3PO_4 nanoparticles onto the TiO_2 surface was achieved by an in situ precipitation method [25]. First, 10 g TiO_2 was dispersed in 50 mL DI water and sonicated for 5 min. Then 3 g $AgNO_3$ was added to the above TiO_2 suspension. Na_3PO_4 solution was prepared by dissolving 2.3 g Na_3PO_4 in 30 mL DI water. Na_3PO_4 solution was subsequently added dropwise to the TiO_2 suspension. The mixture was continuously stirred for 5 h at room temperature; finally, the color of the solution changed from white to yellow. The precipitated solid product (Ag_3PO_4/TiO_2) was then filtered, washed, and dried for subsequent use.

2.3. Fabrication of Ag_3PO_4/TiO_2 blended membranes

Different amounts of TiO_2 and Ag_3PO_4/TiO_2 nanocomposite were uniformly dispersed in the DMF solvent with the aid of sonication. Subsequently, PVDF and PVP were added into the suspensions with the aid of agitation for 4 h to prepare a homogeneous mixture and then degassed at 60°C overnight under negative pressure to remove air bubbles. All the as-synthesized nanocomposite membrane compositions were illustrated in Table 1. The dope solution was casted evenly onto a glass substrate with a casting knife gap of 250 μm. The fresh membrane was transferred into the DI water bath at ambient temperature. A similar casting dope without any blending material was prepared as a control.

Table 1
Composition (wt%) of the different dope solutions for membrane preparation

Membranes	PVDF	PVP	DMF	TiO_2	Ag_3PO_4/TiO_2
P0	18	1.5	80.5	0	0
P1	18	1.5	80.4	0.1	0
P2	18	1.5	80.4	0	0.1
P3	18	1.5	80.2	0	0.3
P4	18	1.5	80.0	0	0.5
P5	18	1.5	79.5	0	1.0

2.4. Characterization of Ag_3PO_4/TiO_2 nanocomposite

The X-ray diffraction (XRD) patterns were recorded using a Y-2000 diffractometer (Bruker AXS D8 Advance, Germany) with monochromatic Cu Kα1 radiation (λ = 1.5406 Å, 40 kV, 20 mA). The 2θ angular regions between 10° and 90° were used to confirm the crystalline structures of TiO_2 and Ag_3PO_4/TiO_2 nanocomposite.

The morphological properties and selected area electron diffraction (SAED) were observed on a JEOL JEM-2100HR transmission electron microscopy (TEM) equipped with an energy-dispersive X-ray spectrometer.

2.5. Characterization of the blended membranes

2.5.1. Structural characterization

The membranes were coated with a conductive platinum film by sputter coating method under vacuum and positioned on a metal holder to investigate the surface morphologies with a ZEISS Ultra 55 field-emission scanning electron microscopy (FE-SEM). The samples for a clear cross-section scanning electron microscope (SEM) images were prepared by a fracture of the dried membranes in liquid nitrogen and then a platinum coating. The XRD patterns were recorded in the 2θ angular regions from 10° to 60° to study the crystalline structures of the nanocomposites.

2.5.2. Separation performance of membrane samples

The water flux of the nanocomposite membranes was carried out using a MSC300 ultrafiltration cup (Shanghai Mosu Science Equipment Co., Ltd., Shanghai, China). The membrane was first filtered with DI water for 40 min at 0.1 MPa until the flux was steady prior to investigating the membrane retention behavior by 1 g/L BSA aqueous solution. BSA concentrations in the feed solution and the permeation were measured by a UV–Vis spectrophotometer (UV-1800, Shimadzu, Kyoto, Japan) at λ_{max} of 280 nm.

The permeate flux (J_w) was calculated using Eq. (1):

$$J_w = \frac{V}{A \times \Delta t} \tag{1}$$

where V is the total volume of permeation (L); Δt was the permeation time (h); and A is the effective membrane area (m^2). The whole experiments were carried out at room temperature.

Then, BSA solution replaced pure water. Finally, the membranes were washed, and the water flux of the cleaned membranes was recorded as J_2 (L/m^2·h). The flux recovery ratio (FRR) and relative flux reduction (RFR) were used to measure antifouling properties of the membrane as shown in Eqs. (2) and (3):

$$\mathrm{FRR} = \frac{J_2}{J_w} \times 100\% \tag{2}$$

$$\mathrm{RFR} = 1 - \frac{J_w}{J_2} \times 100\% \tag{3}$$

The BSA rejection was determined by the ratio the BSA concentration in the feed solution and permeation according to Eq. (4):

$$R\% = \frac{C_f - C_p}{C_f} \times 100\% \tag{4}$$

where C_p and C_f were the concentrations of the permeate and the feed solution, respectively.

The membrane hydrophilicity was characterized by the water contact angle using a contact angle instrument (SL200B, USA KINO Industry Co., Ltd., Norcross, USA). First, a drop of DI water with 5 μL was loaded onto the outer surface of the as-synthesized membrane by a manual microliter syringe. Subsequently, the static water contact angle was measured immediately after taking the droplet image. Finally, the average value of the contact angle was obtained from the measurements of ten different points on each membrane.

The porosity of the nanocomposite membranes was determined by the dry-wet weight method reported elsewhere [26]. The porosity ε (%) of the membranes was determined according to Eq. (5):

$$\varepsilon = \frac{(W_1 - W_2)/\rho_{water}}{(W_1 - W_2)/\rho_{water} + W_2/\rho_{PVDF}} \times 100\% \tag{5}$$

where W_1 is the weight of wet sample; W_2 is the weight of the dry sample; ρ_{water} is the density of pure water; and ρ_{PVDF} is the density of dry state membrane (kg/m^3).

A universal tensile testing machine was utilized to explore tensile strength and elongation at break of the PVDF membranes by under ambient conditions. Each membrane sample with an effective length of 100 mm was tested at a constant uniaxial stretching with a rate of 100 mm/min. An average value from 10 times testing was finally collected.

2.6. Determination of antibacterial activity

2.6.1. Halo zone test

The antibacterial activity of the nanoparticle blended membranes (P1 and P4) and the control membrane P0 were investigated qualitatively using the anti-*E. coli* zone of inhibition test as reported elsewhere [27]. The testing *E. coli* bacteria were first cultivated in 100 mL of a 2.5 wt% yeast-dextrose broth (consisting of 5 g/L yeast extract, 10 g/L sodium chloride, and 10 g/L peptone at a pH of 7.2) at 37°C with shaking at 100 rpm for 24 h. The membrane samples were punched to prepare circular samples with ~2 mm in radius, and 100 μL of the *E. coli* solution (1 × 10^6 cfu/mL) was uniformly spread on the Luria-Bertani (LB) agar plate. The circular membrane specimens were then placed on the surface of treated LB plate and incubated at 37°C for 24 h. The inhibition zone formed after 24 h served as an indicator for the antibacterial activity and was analyzed for growth inhibition.

2.6.2. Bacteria adhesion test

The bacterial adhesion to the surfaces of the control and modified membranes was evaluated by shake flask method.

All membrane specimens were irradiated for sterilization by UV light (300W xenon lamp) for 1 h and pre-soaked in phosphate buffer solution (PBS) prior to immersing into *E. coli* solution. Three pieces 2 × 2 cm^2 of membranes were immersed in 50 mL *E. coli* solution (1 × 10^6 cfu/mL) in a 100-mL sterile Erlenmeyer flask at 37°C and then shaken at 100 rpm for 4 h. Subsequently, the target membranes were drawn out of the *E. coli* solution and gently rinsed three times with PBS. Then the *E. coli* cells on the membrane surfaces were quickly fixed with 2.5% glutaraldehyde in PBS for ~4 h at 4°C. After fixation, the membranes were removed from glutaraldehyde solution and rinsed by PBS buffer six times. Finally, they suffered dehydration by sequential washes in graded ethanol of 30%, 50%, 70%, 90%, and 100% for 10 min. After washing with 100% isoamyl acetate, the membranes were critical point dried with CO_2 so as to observe the quantities and morphologies of bacteria adhered on the membrane surfaces by SEM.

3. Results and discussion

3.1. Structural characterization

Fig. 1 depicts the XRD patterns of pristine TiO_2 and as-synthesized Ag_3PO_4/TiO_2 nanocomposite. The TiO_2 diffraction pattern exhibits sharp peaks at 25.3°, 37.9°, 48.0°, 54.3°, 55.4°, and 63.0°, which correspond to (101), (004), (200), (105), (211), and (204) crystal planes, respectively, indicating a mixture of rutile and anatase phase. In the curve of Ag_3PO_4/TiO_2, there are three obvious peaks centered at 29.8°, 33.3°, and 36.6°, which were in good agreement with the diffractions from the (200), (210), and (211) crystal planes of a body-centered cubic Ag_3PO_4, respectively. The dispersion of Ag_3PO_4 in Ag_3PO_4/TiO_2 nanocomposites was revealed by TEM measurements. It can be clearly seen from Fig. 2 that a lot of dark spots, which present Ag_3PO_4 nanoparticles possessing particle size of 2–8 nm in diameter, were highly dispersed on the surface of TiO_2 with particle diameter ranging from 16 to 50 nm. During the silver impregnation process, Ag^+ was pre-adsorbed onto the TiO_2 surface, and Ag_3PO_4 was thereafter formed due to the reaction of PO_4^{3-} ion with Ag^+. It is noteworthy that SAED rings and points correspond to the TiO_2 multicrystalline phase and Ag_3PO_4 monocrystalline phase, respectively, which is consistent with the previous XRD characterizations. Both XRD patterns and TEM image of Ag_3PO_4/TiO_2 nanocomposites clearly show that the Ag_3PO_4 nanoparticles have been successfully loaded onto the surface of TiO_2 support.

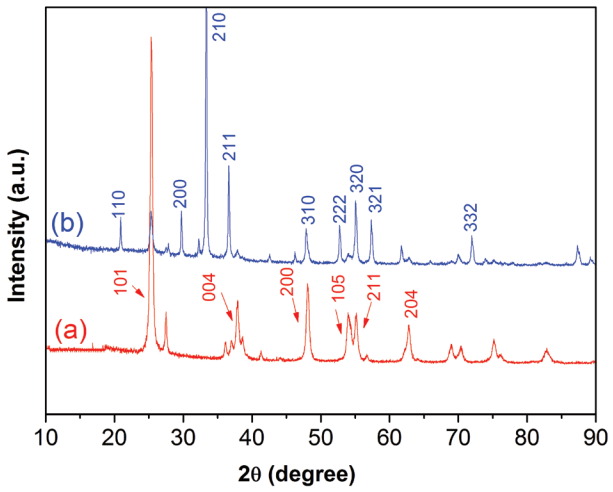

Fig. 1. XRD patterns of the pristine TiO_2 (a) and as-prepared Ag_3PO_4/TiO_2 nanocomposites (b).

Fig. 3 depicts the top-view and cross-sectional SEM images of the nanoparticle blended nanocomposite

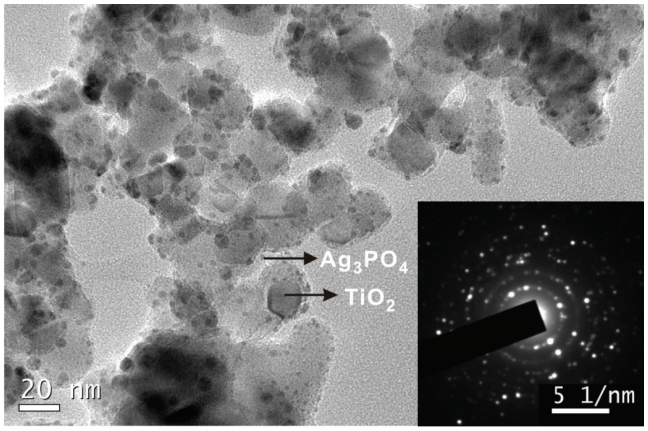

Fig. 2. The TEM image of Ag_3PO_4/TiO_2 nanocomposites. The inset shows the SAED image of Ag_3PO_4/TiO_2 nanocomposites.

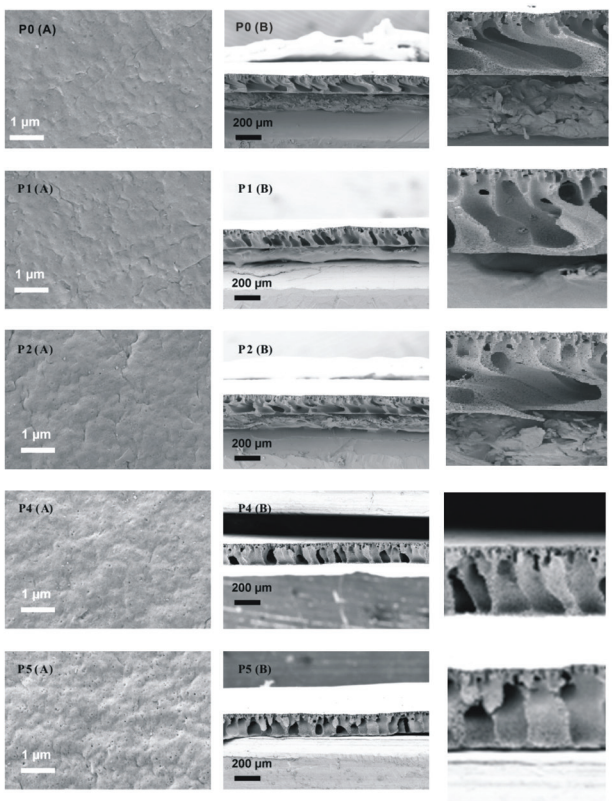

Fig. 3. Top-view (A) and cross-sectional (B) FE-SEM images of the control (P0) and modified membranes (P1, P2, P4, P5); right column is the enlarged cross-sectional images.

membranes (P1, P2, P4, and P5) and the control membrane (P0). As shown in Fig. 3(A), the nanocomposite membranes (P1 and P2) is of flat and smooth features on the top surface, which is similar to that of pristine control membrane (P0). From P2 to P5, it is obvious that the increased concentration of Ag_3PO_4/TiO_2 nanocomposites in the casting solution resulted in rougher surface with more fully developed macropores on the top side of modified membranes. It could be attributed to the aggregation of the nanoparticles on the surface when their concentration is high. As the casted PVDF dope solution on the glass substration was immersed into the water bath for coagulation, a non-solvent/solvent exchange immediately occurred across the interface between the non-solvent and casting film. Therefore, the near-surface nanocomposites dispersed in solvent may serve as pore-forming agent. The repulsive forces between water and PVDF together with the fast non-solvent/solvent interchange caused an immediate PVDF precipitation at the interface. Consequently, a typical asymmetric structure composed of well-developed macrovoids and finger-like pores connected by sponge walls in sub-layer was formed.

Fig. 4 presents the XRD patterns of PVDF–Ag_3PO_4/TiO_2 composite membranes and pristine PVDF membrane. There are two characteristic peaks of PVDF crystal at 2θ of 18.5° and 20.1°, which correspond to the planes of (100) and (020), respectively. After incorporating TiO_2 and Ag_3PO_4/TiO_2 into the PVDF matrix, no characteristic peaks of TiO_2 and Ag_3PO_4/TiO_2 nanoparticles were observed in the XRD patterns that could be contributed by the embedment of Ag_3PO_4/TiO_2 in matrix by polymer chains or a high compatibility between PVDF and blending materials from phase inversion process [28].

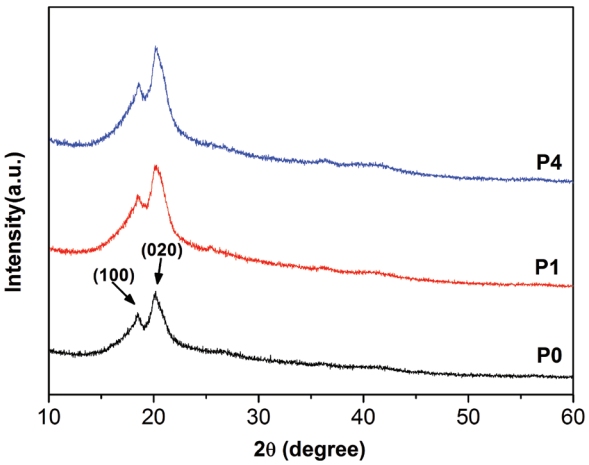

Fig. 4. XRD patterns of the pristine membrane (P0) and modified membranes (P1 and P4).

Table 2
Contact angle, mechanical property, and porosity of the membranes

Membrane	Contact angle (°)	Tensile strength (MPa)	Breakage elongation (%)	Porosity (%)
P-0	76.05 ± 1.18	1.59	22.42	84.67 ± 0.72
P-1	67.01 ± 1.43	1.67	30.26	84.66 ± 0.63
P-2	66.70 ± 2.01	1.61	29.50	84.75 ± 0.50
P-3	67.56 ± 2.31	1.98	31.77	84.79 ± 0.82
P-4	64.95 ± 2.37	1.80	30.33	84.92 ± 0.43
P-5	63.46 ± 2.21	1.69	29.89	85.05 ± 0.51

3.2. Mechanical strength, contact angle, and separation performance of membrane samples

Table 2 summarizes all as-prepared membrane properties with respect to their porosity, contact angle, mechanical strength, and breakage elongation. Normally, blending TiO_2 nanoparticles would be expected to significantly increase membrane porosity [29], but the membrane porosity was slightly affected by the blending materials of Ag_3PO_4/TiO_2 in this study as all the membranes prepared displayed reasonably high porosity ranging from 84.67% to 85.05%, which is in accordance with the results elsewhere [30]. There is no controversy that high membrane porosity was dominantly contributed by the presence of hydrophilic PVP with high molecular weight in dope solution regardless of the Ag_3PO_4/TiO_2 concentration due to the occurrence of solution demixing induced by PVP and enhancement of phase separation [31]. Mechanical properties are extremely important for PVDF membranes as the membranes breaking will lose separation performances. As shown in Table 2, with respect to mechanical strength and breakage elongation, all PVDF membranes incorporated with blending nanoparticles demonstrated greater mechanical strength compared with that of pristine membrane. The tensile strength and breakage elongation gradually reach a maximum of 1.98 MPa and 31.77% when adding 0.3 wt% Ag_3PO_4/TiO_2 nanocomposite and then successively drop down as further increasing of the loadings of Ag_3PO_4/TiO_2. These results revealed that blending appropriate amount of Ag_3PO_4/TiO_2 in PVDF dope solution can enhance the mechanical properties of the resultant nanocomposite membranes, which is consistent with the results elsewhere the literature [32,33]. The variation of the membrane hydrophobicity caused by the casting mixture composition was investigated by the water contact angle measurements. When the weight ratio of Ag_3PO_4/TiO_2 was successively increased up to 1 wt%, a gradual decreasing in membrane contact angle from 76.05° to 63.46° was observed since the surface of TiO_2 was abundant with oxygenated hydrophilic groups and therefore enhanced surface hydrophilicity.

As shown in Fig. 5, the pristine membrane exhibits a minimum permeate water flux of 47.15 L/m²·h and a maximum BSA rejection of 91.1%. As the addition of TiO_2 and Ag_3PO_4/TiO_2, a remarkable improvement in permeate water flux from 57.35 to 103.72 L/m²·h was observed for the modified membranes, whereas a plateaus of BSA rejection around 83.5% was maintained from P1 to P4 membranes until a sudden drop occurred for P5 samples because of a higher porosity. Apparently, the trend of an enhancement in water flux was complied with that of the surface hydrophilicity and water contact angle. It is universally acknowledged that an improvement in surface hydrophilicity of the nanoparticle blended nanocomposite membranes has a favorable effect on

the water flux via attracting water molecules inside the modified PVDF membrane matrix and therefore facilitating their permeation across the blended membrane.

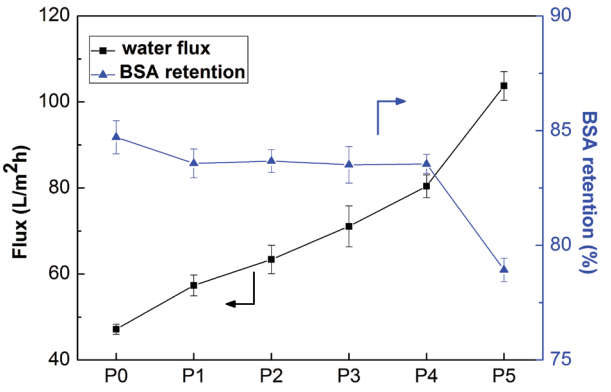

Fig. 5. Water flux (0.1 MPa) and the rejection of BSA of the PVDF membranes made with different TiO_2 and Ag_3PO_4/TiO_2 content.

3.3. Antifouling performance and antibacterial activity

Rate of flux decline, RFR, and FRR are employed to evaluate the antifouling ability of the membranes. As shown in Fig. 6, Ag_3PO_4/TiO_2 blended membranes exhibit lower rate of flux decline compared with 33.34% for the unmodified membrane and higher FRR. P4 membrane shows the lowest rate of flux decline (14.35%) and RFR (8.77%), and the highest FRR (91.23%). The antibacterial property of the Ag_3PO_4/TiO_2 modified membranes against *E. coli* was characterized using the halo testing. Ag_3PO_4 nanoparticle has been found to be a significant antibacterial material due to slow-released silver ions that could attach to the cell membrane and then interact with the DNA or protein macromolecules in the cell to interfere or impede vital metabolic processes. As shown in Fig. 7(a), it is noticeably found that P0 and P1 membranes has no inhibitive ability on the *E. coli* bacterial owning to the absence of the zone of inhibition. In contrast, a remarkable zone of inhibition without bacterial growth was observed surrounding the P2 membrane. A zone width is of ~2 mm clearly indicated P2 membrane had a promising antibacterial activity against *E. coli* and Ag_3PO_4/TiO_2 blending was able

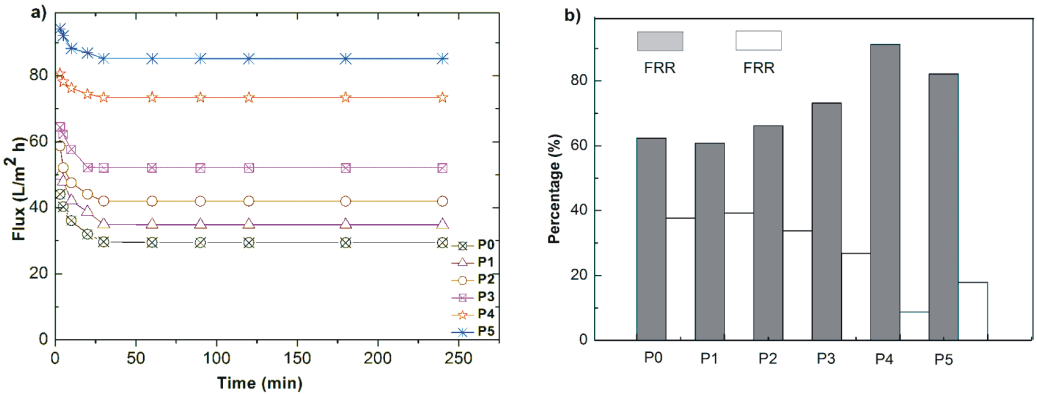

Fig. 6. (a) Permeate flux decline with increasing time for control membrane (P0) and modified membranes and (b) relative flux reduction (RFR) and flux recovery ratio (FRR) of control membrane (P0) and modified membranes (P1, P2, P4, P5).

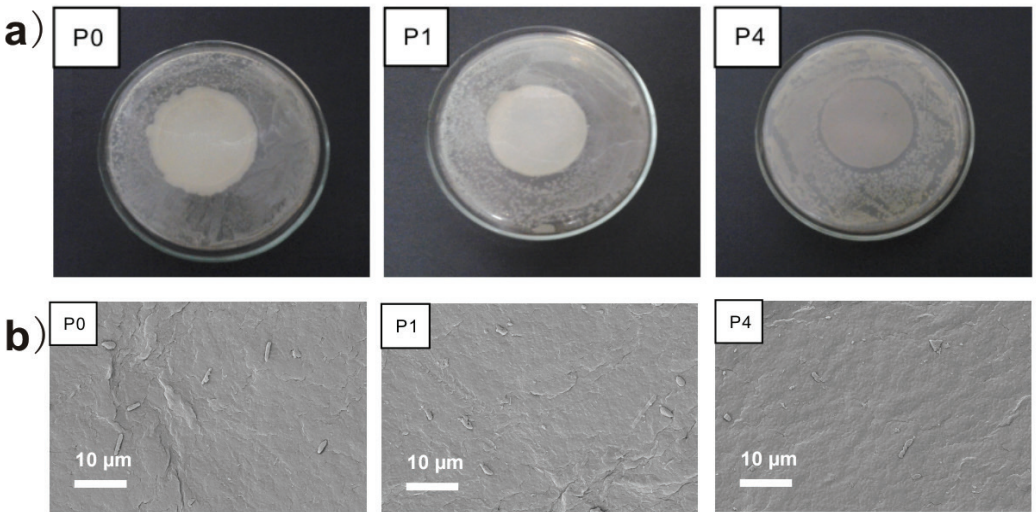

Fig. 7. (a) Measurement of the antibacterial property of P0, P1 and P4 membranes using the halo zone test and (b) FE-SEM images of the bacteria adhered on the membrane surfaces.

to improve the antifouling behavior of the modified PVDF nanocomposite membranes.

The bacterial colonies derived membrane fouling could be induced by the bacteria accumulation and adhesion on the membrane surface [34]. To investigate the *E. coli* adhesion on membranes, SEM was employed to study the quantities and morphology of cells on surface of the membranes. As shown in Fig. 7(b), Ag_3PO_4/TiO_2 blended P4 membrane were found to have much less rod-shaped bacterial adherence to the surfaces compared with P0 and P1 membranes. Moreover, the *E. coli* on P4 membrane displayed an obviously deformed shape. The *E. coli* attachment results indicate that P4 membrane had a better antiadhesive activity against *E. coli* owing to the slow-released Ag^+ and expectedly had a greater potential in antifouling.

4. Conclusions

Hydrophilic and antibacterial membranes were successfully synthesized with wet phase inversion method by blending Ag_3PO_4/TiO_2 nanocomposite. Results revealed that Ag_3PO_4/TiO_2 blended membranes showed higher tensile strength and breakage elongation. The water flux was dramatically increased with the addition of Ag_3PO_4/TiO_2 in dope solution. P4 membrane doped with 0.5 wt% Ag_3PO_4/TiO_2 exhibits an enhanced permeate water flux of 80.41 $L/m^2 \cdot h$ while high BSA rejection remains nearly unchanged due to synchronously increased hydrophilicity. Moreover, P4 membrane has a tensile strength of 1.80 MPa and 30.33% elongation implying its potential application as an ultrafiltration membrane. FE-SEM images indicated that the degree of *E. coli* cells adhesion to the membrane surface was markedly reduced with blending Ag_3PO_4/TiO_2. Meanwhile, the halo zone tests also implied that P4 membrane had an obvious antibacterial activity against *E. coli*. In conclusion, Ag_3PO_4/TiO_2 blended PVDF nanocomposite membrane is of good separation performance while possessing a good antibacterial behavior and a high fouling resistance.

Acknowledgments

Financial support for this work was provided by the National Nature Science Foundation of China (21203067), Zhejiang University of Science and Technology youth talent cultivation plan, Major Science and Technology Projects of Zhejiang province (2015C02037), and National Keypoint Research and Invention Program (China 13th Five Year Plan, 2017YFD061000).

References

[1] H.K. Oh, J.Y. Eom, S.H. Kang, B.G. Lee, H.C. Yoo, B.O. Lee, A study on enhancing physical cleaning effectiveness in microfiltration membrane system, Desal. Wat. Treat., 54 (2015) 3596–3602.

[2] A. Ali, P. Aimar, E. Drioli, Effect of module design and flow patterns on performance of membrane distillation process, Chem. Eng. J., 277 (2015) 368–377.

[3] L. Francis, N. Ghaffour, A.S. Alsaadi, S.P. Nunes, G.L. Amy, PVDF hollow fiber and nanofiber membranes for fresh water reclamation using membrane distillation, J. Mater. Sci., 49 (2014) 2045–2053.

[4] A.W. Qin, X. Li, X.Z. Zhao, D.P. Liu, C.J. He, Preparation and characterization of nano-chitin whisker reinforced PVDF membrane with excellent antifouling property, J. Membr. Sci., 480 (2015) 1–10.

[5] W. Li, H. Li, Y.-M. Zhang, Preparation and investigation of PVDF/PMMA/TiO_2 composite film, J. Mater. Sci., 44 (2009) 2977–2984.

[6] Y.C. Woo, J.J. Lee, L.D. Tijing, H.K. Shon, M.W. Yao, H.S. Kim, Characteristics of membrane fouling by consecutive chemical cleaning in pressurized ultrafiltration as pre-treatment of seawater desalination, Desalination, 369 (2015) 51–61.

[7] T. Bohli, A. Ouederni, N. Fiol, I. Villaescusa, Evaluation of an activated carbon from olive stones used as an adsorbent for heavy metal removal from aqueous phases, C.R. Chim., 18 (2015) 88–99.

[8] X.S. Yi, S.L. Yu, W.X. Shi, N. Sun, L.M. Jin, S. Wang, B. Zhang, C. Ma, L.P. Sun, The influence of important factors on ultrafiltration of oil/water emulsion using PVDF membrane modified by nano-sized TiO_2/Al_2O_3, Desalination, 281 (2011) 179–184.

[9] N.A. Hashim, F. Liu, M.R.M. Abed, K. Li, Chemistry in spinning solutions: surface modification of PVDF membranes during phase inversion, J. Membr. Sci., 415 (2012) 399–411.

[10] S. Wongchitphimon, R. Wang, R. Jiraratananon, Surface modification of polyvinylidene fluoride-co-hexafluoropropylene (PVDF-HFP) hollow fiber membrane for membrane gas absorption, J. Membr. Sci., 381 (2011) 183–191.

[11] M. Safarpour, A. Khataee, V. Vatanpour, Effect of reduced graphene oxide/TiO_2 nanocomposite with different molar ratios on the performance of PVDF ultrafiltration membranes, Sep. Purif. Technol., 140 (2015) 32–42.

[12] J.H. Li, B.F. Yan, X.S. Shao, S.S. Wang, H.Y. Tian, Q.Q. Zhang, Influence of Ag/TiO_2 nanoparticle on the surface hydrophilicity and visible-light response activity of polyvinylidene fluoride membrane, Appl. Surf. Sci., 324 (2015) 82–89.

[13] S. Liang, K. Xiao, Y.H. Mo, X. Huang, A novel ZnO nanoparticle blended polyvinylidene fluoride membrane for anti-irreversible fouling, J. Membr. Sci., 394 (2012) 184–192.

[14] F. Liu, M.R.M. Abed, K. Li, Preparation and characterization of poly(vinylidene fluoride) (PVDF) based ultrafiltration membranes using nano γ-Al_2O_3, J. Membr. Sci., 366 (2011) 97–103.

[15] X.S. Yi, W.X. Shi, S.L. Yu, C. Ma, N. Sun, S. Wang, L.M. Jin, L.P. Sun, Optimization of complex conditions by response surface methodology for APAM-oil/water emulsion removal from aqua solutions using nano-sized TiO_2/Al_2O_3 PVDF ultrafiltration membrane, J. Hazard. Mater., 193 (2011) 37–44.

[16] H.Q. Liang, Q.Y. Wu, L.S. Wan, X.J. Huang, Z.K. Xu, Thermally induced phase separation followed by in situ sol-gel process: a novel method for PVDF/SiO_2 hybrid membranes, J. Membr. Sci., 465 (2014) 56–67.

[17] J.P. Mericq, J. Mendret, S. Brosillon, C. Faur, High performance PVDF-TiO_2 membranes for water treatment, Chem. Eng. Sci., 123 (2015) 283–291.

[18] A.W. Qin, X. Li, X.Z. Zhao, D.P. Liu, C.J. He, Engineering a highly hydrophilic PVDF membrane via binding TiO_2 nanoparticles and a PVA Layer onto a membrane surface, ACS Appl. Mater. Interfaces, 7 (2015) 8427–8436.

[19] S. Qiu, X. Huang, S. Xu, F. Ma, The antibacterial activity of ceramsite coated by silver nanoparticles in micropore, Appl. Biochem. Biotechnol., 176 (2015) 267–276.

[20] X.C. Cao, J. Ma, X.H. Shi, Z.J. Ren, Effect of TiO_2 nanoparticle size on the performance of PVDF membrane, Appl. Surf. Sci., 253 (2006) 2003–2010.

[21] R.A. Damodar, S.J. You, H.H. Chou, Study the self cleaning, antibacterial and photocatalytic properties of TiO_2 entrapped PVDF membranes, J. Hazard. Mater., 172 (2009) 1321–1328.

[22] S.J. Oh, N. Kim, Y.T. Lee, Preparation and characterization of PVDF/TiO_2 organic-inorganic composite membranes for fouling resistance improvement, J. Membr. Sci., 345 (2009) 13–20.

[23] M.T. Moghadam, G. Lesage, T. Mohammadi, J.P. Mericq, J. Mendret, M. Heran, C. Faur, S. Brosillon, M. Hemmati, F. Naeimpoor, Improved antifouling properties of TiO_2/PVDF nanocomposite membranes in UV-coupled ultrafiltration, J. Appl. Polym. Sci., 132 (2015) 15.

[24] X. Li, R.Z. Pang, J.S. Li, X.Y. Sun, J.Y. Shen, W.Q. Han, L.J. Wang, In situ formation of Ag nanoparticles in PVDF ultrafiltration

membrane to mitigate organic and bacterial fouling, Desalination, 324 (2013) 48–56.
[25] W.F. Yao, B. Zhang, C.P. Huang, C. Ma, X.L. Song, Q.J. Xu, Synthesis and characterization of high efficiency and stable Ag_3PO_4/TiO_2 visible light photocatalyst for the degradation of methylene blue and rhodamine B solutions, J. Mater. Chem., 22 (2012) 4050–4055.
[26] C.J. Liao, P. Yu, J.Q. Zhao, L.M. Wang, Y.B. Luo, Preparation and characterization of NaY/PVDF hybrid ultrafiltration membranes containing silver ions as antibacterial materials, Desalination, 272 (2011) 59–65.
[27] M.Y. Zhang, K.S. Zhang, B. De Gusseme, W. Verstraete, Biogenic silver nanoparticles (bio-Ag^0) decrease biofouling of bio-Ag^0/PES nanocomposite membranes, Water Res., 46 (2012) 2077–2087.
[28] Z.K. Li, W.Z. Lang, W. Miao, X. Yan, Y.J. Guo, Preparation and properties of PVDF/SiO_2@GO nanohybrid membranes via thermally induced phase separation method, J. Membr. Sci., 511 (2016) 151–161.
[29] Q.Y. Wang, Z.W. Wang, J. Zhang, J. Wang, Z.C. Wu, Antifouling behaviours of PVDF/nano-TiO_2 composite membranes revealed by surface energetics and quartz crystal microbalance monitoring, RSC Adv., 4 (2014) 43590–43598.
[30] C.S. Ong, W.J. Lau, P.S. Goh, B.C. Ng, A.F. Ismail, Preparation and characterization of PVDF-PVP-TiO_2 composite hollow fiber membranes for oily wastewater treatment using submerged membrane system, Desal. Wat. Treat., 53 (2015) 1213–1223.
[31] Z. Yuan, X. Dan-Li, Porous PVDF/TPU blends asymmetric hollow fiber membranes prepared with the use of hydrophilic additive PVP (K30), Desalination, 223 (2008) 438–447.
[32] S. Majeed, D. Fierro, K. Buhr, J. Wind, B. Du, A. Boschetti-De-Fierro, V. Abetz, Multi-walled carbon nanotubes (MWCNTs) mixed polyacrylonitrile (PAN) ultrafiltration membranes, J. Membr. Sci., 403 (2012) 101–109.
[33] W.Z. Lang, Q. Ji, J.P. Shen, Y.J. Guo, L.F. Chu, Modified poly(vinylidene fluoride) hollow fiber composite membranes reinforced by hydroxyapatite nanocrystal whiskers, J. Appl. Polym. Sci., 127 (2013) 4564–4572.
[34] F. Yao, G.D. Fu, J.P. Zhao, E.T. Kang, K.G. Neoh, Antibacterial effect of surface-functionalized polypropylene hollow fiber membrane from surface-initiated atom transfer radical polymerization, J. Membr. Sci., 319 (2008) 149–157.